PCCP

PAPER

View Article Online
View Journal | View Issue

Cite this: *Phys. Chem. Chem. Phys.*, 2019, **21**, 2755

Charge-transfer state dynamics in all-polymer solar cells: formation, dissociation and decoherence

Jiaqing Huang, Yijie Mo and Yao Yao *

Received 17th October 2018,
Accepted 30th December 2018

DOI: 10.1039/c8cp06467a

rsc.li/pccp

All-polymer solar cells have made substantial achievements in recent years, offering numerous unsettled subjects for mechanical researchers. In order to quantitatively study the influence of the molecular electrostatic potential on the charge generation proposed by the experimenter, we simulate the ultrafast dynamics of the charge-transfer (CT) state at the interface between two polymer chains, which are respectively regarded as the donor and acceptor in all-polymer solar cells. The formation of a stable CT state is found to be sensitive to the distance between two oppositely charged polarons and the relevant critical electrostatic potential is thus quantified, which is in good agreement with experiments. In order to get insight into the dependence of the dissociation of the CT state on the width of the interfacial layer, two quantities are calculated: one is the Coulomb capture radius between the two polarons and the other is the quantum trace distance which serves as the fingerprint of the quantum coherence between them. The dissociation of the CT state is found to take place within an ultrafast timescale for an optimum interfacial width. The classical spatial distance and the quantum trace distance manifest a converging trend, suggesting a decoherence scenario for the charge separation in all-polymer solar cells.

I. Introduction

Following the rapid developing progress of non-fullerene organic solar cells (OSCs),[1–3] all-polymer solar cells (all-PSCs) emerged as novel candidates with perfect performance and environmental friendliness.[4–8] All-PSCs employ conjugated polymers with strong electron-withdrawing ability, such as the naphthalenediimide (NDI) polymer N2200,[6–11] as the electron acceptor, which are qualitatively distinct from the conventional fullerene-based acceptors. They exhibit the advantages of tenability of electronic structure, enhanced light absorption, and superior mechanical and thermal properties.[12–14] The up-to-date power conversion efficiency (PCE) of all-PSCs has increased over 11%,[15] benefitting from the optimized design of polymeric materials as electron acceptors and the dramatic development of the device processing technology since all-PSCs were first reported in 1995.[16]

The study of the formation and efficient dissociation of the Frenkel excitons is crucial for understanding the working mechanisms of OSCs. The Frenkel exciton is conventionally regarded to be the initial local excited state after photoexcitation, which possesses the characteristics of a tightly-bound electron–hole pair with large binding energy induced by both the self-trapping effect and the Coulomb attraction.[17–19] It is desired that these excitons efficiently dissociate into free charge carriers in order to generate a sufficiently large photocurrent. Nevertheless, an intermediate state composed of a weakly-bound electron–hole pair with the electron and the hole being respectively coupled to their own local lattice distortion, which is also called the charge-transfer (CT) state (or the polaron-pair state),[20–24] is formed across the donor/acceptor (D/A) interface instead of the direct formation of free charge carriers. In traditional fullerene-based cells, the conversion from the Frenkel exciton to the CT state is determined by the relative relation between the exciton binding energy, ε_B, and the energy (ionization potential) offset, ΔE, between donor and acceptor.[24–27] If ΔE is greater than ε_B, the photogenerated Frenkel exciton will be transformed into a CT state owing to the energy instability; otherwise, the Frenkel exciton will remain stable and the dissociation taking place will be unlikely.

In non-fullerene solar cells, however, experiments have shown that the energy offset does not matter in the process of charge separation.[28,29] Unlike the traditional fullerene-based cells in which a significant energy offset ($\sim$0.3 eV)[19,25,26,30] is necessary for charge separation, non-fullerene cells enable fast and efficient charge separation despite the negligible energy offset ($\sim$0.05 eV). Liu *et al.* reported a non-fullerene OSC with the PCE being 9.5% based on the P3TEA:SF-PDI$_2$ blend,[28] and Nikolis *et al.* obtained a high external quantum efficiency (EQE) of 79% based on the α-6T/SubNc non-fullerene OSC.[29]

Department of Physics and State Key Laboratory of Luminescent Materials and Devices, South China University of Technology, Guangzhou 510640, China. E-mail: yaoyao2016@scut.edu.cn

Both their devices were observed to have a small driving force, which results in the low open-circuit voltage loss and thus improves the device efficiency. In this context, the current interest of the emerging non-fullerene OSCs is focusing on the following questions: is there still an intermediate state such as the CT state in the process of charge separation, and what then serves as the driving force therein?

The dissociation of the CT state has been widely investigated for a long time and many experimental and theoretical results for this process have been reported.[31–41] The energetic disorder was a crucial point in early investigations, and based on the hopping transport model the field-assisted dissociation of the CT state was proposed in the disordered systems.[31] The surface losses due to CT state diffusion were taken into account for the dissociation efficiency of the CT state.[32] By comparison, the critical effects of charge delocalization and entropy increase were highlighted in the process of CT state dissociation.[33–37] More recently, the molecular packing, orientation and blend morphology were also reported to play important roles in CT state dissociation and charge separation.[13,38–40] Despite this research, the underlying mechanism of the dissociation of the CT state is still hotly debated. Hou's group recently proposed a novel mechanism based upon the molecular electrostatic potential (ESP).[41] They stated that the intermolecular electric field resulting from the difference in the molecular ESPs between donor and acceptor materials facilitated efficient charge separation at the D/A interface in non-fullerene cells. The present work is thus motivated to quantify the influence of molecular ESPs on the charge separation in a theoretical manner. Our objective is to establish a quantitative indicator for this issue to help experimenters understand their measurements.

In recent works, one of the authors studied the charge transfer and separation in small-molecule OSCs, in which the long-range charge transfer state was highlighted.[42–44] On the other side, herein, the discussion of all-PSCs is presented. Two components of the polymer chain are set head-to-tail to construct the D/A interface and a molecular ESP drop is involved in the modeling. The formation and the dynamic dissociation of the CT state at the D/A interface are investigated within the framework of the Su–Schrieffer–Heeger (SSH) model.[45] The conditions for the existence of a stable CT state will be discussed, and the separation process of the two polarons in the CT state will be featured by the spatial distance, as well as the quantum trace distance which is in our view more important than the former one. The paper is organized in the following sequence. The model and method are given in Section II. The results and discussion are presented in Section III. Finally in Section IV, the main conclusions are drawn.

II. Model and method

Based on recent experimental works,[46–51] we took a representative J51/N2200 blend introduced by Li's group[6] as an example to study the CT dynamics of all-PSCs. In this blend, the electron donor is J51, which is a copolymer donor with two cores, benzodithophene and benzotriazole, polymerized by two thiophene rings. The benzotriazole group possesses strong electron affinity to act as the source of self-doping, and the benzodithophene and two thiophene rings provide conjugated orbitals for the electron transport. The electron acceptor in the blend, N2200, also adopts thiophene rings to polymerize the NDI cores. NDI is a derivative of naphthalene, which has good electron conductivity. Radicals on the imide end groups in NDI have also got strong electron affinity, and electrons can be self-doped into the backbone formed by naphthalene and thiophenes. The alkyl groups behave as side groups to improve solubility and form a perfect one-dimensional (1D) polymer chain.

Different from those in small molecules, the carriers in polymers are attributed to large polarons. The CT state in polymers is also formed by the intermolecular polaron pairs on different polymer chains. The large polaron is a topological elementary excitation which can only be described by the benchmarking SSH model or its alternates. In this model, the vibrations are treated as topological deformations of the functional moieties instead of the quantized phonons. The π-conjugated orbitals on the thiophene, benzodithophene and naphthalene backbone provide the transport sites for the self-doped electrons from imide groups and other radicals. In order to study the D/A interface, two polymer chains with different electron affinities (molecular ESPs) are placed head-to-tail.

The total model Hamiltonian then consists of three terms and has the following form:

$$H = H_{\mathrm{SSH}} + H_{\mathrm{U}} + H_{\mathrm{P}}. \tag{1}$$

Herein, the first term represents the original SSH Hamiltonian, which contains two parts,

$$H_{\mathrm{SSH}} = H_{\mathrm{ele}} + H_{\mathrm{lat}}. \tag{2}$$

H_{ele} in eqn (2) is the Hamiltonian of electrons expressed as

$$H_{\mathrm{ele}} = -\sum_{n} t_n\left(\hat{c}_{n+1}^{\dagger}\hat{c}_n + \mathrm{h.c.}\right), \tag{3}$$

where $\hat{c}_n^{\dagger}$ ($\hat{c}_n$) creates (annihilates) an electron on the n-th site and the vibronic coupling is involved in the nearest-neighbor hopping integral t_n given by

$$t_n = t_0 - \alpha(u_{n+1} - u_n), \tag{4}$$

with t_0 being the hopping constant, α the vibronic coupling strength and u_n the displacement of n-th thiophene unit. The second term in eqn (2) represents the elastic potential and kinetic energy of moieties on the backbone, that is

$$H_{\mathrm{lat}} = \frac{K}{2}\sum_{n}(u_{n+1} - u_n)^2 + \frac{M}{2}\sum_{n}\dot{u}_n^2, \tag{5}$$

with K being the elastic constant and M being the mass of the moieties. The second term of eqn (1) is for the many-body electron coupling, which quantifies the coupling between the electron and hole, and the form is

$$H_{\mathrm{U}} = U\sum_{n}\hat{c}_{n,\uparrow}^{\dagger}\hat{c}_{n,\uparrow}\hat{c}_{n,\downarrow}^{\dagger}\hat{c}_{n,\downarrow}, \tag{6}$$

where U gives the strength of the Coulomb interactions. This term will be treated with the Hartree–Fock approximation in the calculations. As the critical consideration of this work, the third term of eqn (1) is the on-site energy V_n denoting the different electron affinities (molecular ESPs) of donor and acceptor, *i.e.*,

$$H_{\mathrm{P}} = \sum_n V_n \hat{c}_n^{\dagger} \hat{c}_n. \tag{7}$$

In order to make the change of V_n across the interface smooth, an analytic form is set as

$$V_n = \frac{V_0}{2}\left[\tanh\frac{4a_0(n-n_0)}{W} + 1\right], \tag{8}$$

where V_0 is the potential drop between donor and acceptor, n_0 is set to the central site of the chain, W is the width of the interfacial layer and a_0 is the lattice constant. Fig. 1 displays the spatial distribution of V_n with the total site number being 300. The donor component of the chain is labeled from 1 to 150 and the remnant is appointed to be the acceptor component. It is reported that the optimized active layer thickness is often limited at around 100 nm in experiments, and an optimized layer thickness of 120 nm was obtained for the J51/N2200 cells[6] and the PTzBI/N2200 cells.[7] Without loss of generality, we made a simple assumption that the conjugation length of the polymers was close to the layer thickness, so we set the chain to have 300 lattice sites (or $\sim$117 nm). There is an interfacial layer between these two components that we can call the D/A interface. V_0 and W determine the electric field strength induced by the potential drop, and obviously at the center of the interface, the electric field is the strongest. It is noted that, the analytic form in eqn (8) is not necessary to be the hyperbolic tangent function and the following results are not sensitive to this specific choice.

Model parameters of the total Hamiltonian have been worked out using our quantum chemistry computations. In all the simulations, we took parameters of the J51/N2200 blend which were set as follows:[52] t_0 = 0.09 eV, α = 3.4 eV Å^{-1}, K = 231 eV Å^{-2}, M = 8509.96 eV fs Å^{-2} and a_0 = 3.9 Å. Our simulating results can be quantitatively compared to the experiments with similar blends. In order to be specific in discussing the interfacial effect, we did not consider the disorder which may promote the dissociation of the CT state in low electric fields.[31]

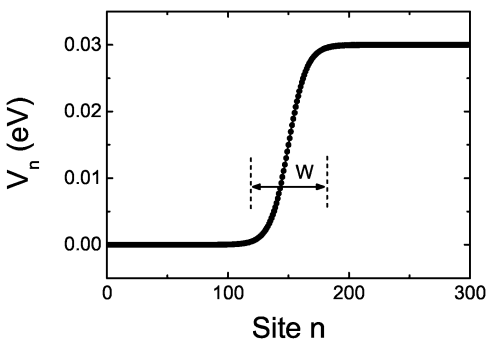

Fig. 1 The spatial distribution of the on-site energy V_n. W is the width of the interfacial layer.

Different from the quantized phonon systems which can be treated using DMRG, MCTDH, HEOM[53] and other approaches, the topological deformation is optimally dealt with using the following procedure of the non-adiabatic dynamic method, which has been proven to be valid in dealing with polaron dynamics in conjugated polymers.[23,54–59] Firstly, the time evolution of the electronic wave function is described with the time-dependent Schrödinger equation:

$$\mathrm{i}\hbar\frac{\partial\psi_{\mu,n}(t)}{\partial t} = -t_n\psi_{\mu,n+1}(t) - t_{n-1}\psi_{\mu,n-1}(t), \tag{9}$$

with $\psi_{\mu,n}$ being the μ-th eigen-state of the Hamiltonian (1) on the n-th site. The solution of this time-dependent Schrödinger equation is formally written as

$$\psi_\mu(t) = \hat{T}\ \exp\left[-\frac{i}{\hbar}\int_0^t \mathrm{d}t' H(t')\right]\psi_\mu(0), \tag{10}$$

where $\hat{T}$ denotes the time ordering operator. In order to obtain the numerical solution of the electronic wavefunction, the integrate time step Δt must be set to be sufficiently small, namely below the order of the bare phonon frequency, $\omega_{\mathrm{Q}} = \sqrt{4K/M}$. Throughout this work, we set it to 0.2 fs. The equation is then rewritten as

$$\psi_\mu(t_{j+1}) = \exp[-\mathrm{i}H(t_j)\Delta t/\hbar]\psi_\mu(t_j). \tag{11}$$

This equation can be alternatively expressed using the instantaneous eigenfunctions, φ_ν, and eigenvalues, ε_ν, of the Hamiltonian, $H(t_j)$, *i.e.*,

$$\psi_\mu(t_{j+1}) = \sum_\nu \left\langle \varphi_\nu|\psi_\mu(t_j)\right\rangle \exp[-\mathrm{i}\varepsilon_\nu\Delta t/\hbar]\varphi_\nu. \tag{12}$$

The motion of the moiety is described as:

$$\begin{aligned} F_n(t) = M\ddot{u}_n = &-K[2u_n - u_{n+1} - u_{n-1}] \\ &+ \alpha[\rho_{n,n+1} - \rho_{n-1,n} + \rho_{n+1,n} - \rho_{n,n-1}], \end{aligned} \tag{13}$$

where $F_n(t)$ is the force exerted on the n-th site and the density matrix ρ is given by

$$\rho_{n,n'} = \sum_\mu \psi^*_{\mu,n}(t) f_\mu \psi_{\mu,n'}(t), \tag{14}$$

with f_μ being the time-independent distribution function. In order to produce the topological elementary excitations such as polarons on the polymer chain, f_μ must be carefully chosen to be 0, 1 or 2 to reflect the occupation of the energy levels of the single-partite system. In our case, specifically, we even have to carefully examine the different occupations of the two chains as we are considering the CT state at the interface. With these considerations, the lattice displacement $u_n(t_{j+1})$ and the velocity $\dot{u}_n(t_{j+1})$ can then be obtained with the following forms:

$$u_n(t_{j+1}) = u_n(t_j) + \dot{u}_n(t_j)\Delta t, \tag{15}$$

$$\dot{u}_n(t_{j+1}) = \dot{u}_n(t_j) + \frac{F_n(t_j)}{M}\Delta t. \tag{16}$$

In this work, we did not study the instantaneous processes of photoexcitation, emission and conversion from exciton to CT state. The dynamics we considered merely take place on one

potential surface, so that the conical cross of surfaces for different states does not matter. It is also worth noting that when the conversion processes between states were investigated, the conical cross played an irreducible role, which is held as our future subject.

III. Results and discussion

We first discuss the formation of the CT state. To this end, the simulating procedure is specifically modified. We first calculate the ground state of the entire system, and then a π-electron is excited from the highest occupied molecular orbital (HOMO) to the lowest unoccupied molecular orbital (LUMO), which mimics the process resulting from the photoexcitation under realistic conditions. *Via* this manipulation, we can obtain either a Frenkel exciton or a CT state. In order to focus on the latter, we artificially put two self-trapping potential valleys (lattice distortions) in the system to induce two oppositely charged polarons, one of which is put in the donor and the other in the acceptor. The initial distance between the two valleys could be realized as the size of the CT state. Through the subsequent procedure of energy optimization for the entire system, the two polarons keep stable in some cases as discussed below, so that we can say the CT state robustly constitutes the excited state after photoexcitation, otherwise the CT state does not emerge as a photoexcited state.

During the generation and dissociation process of the CT state, the description of the motion of the two oppositely charged polarons requires us to define the charge center of a polaron. Considering that there are breathers along with the polaron, the charge center cannot be directly determined by the peak values or the simple average of ρ_n. Therefore, the charge center of the polaron is defined with the following form:

$$x_c = \begin{cases} L\theta/2\pi, & \text{if} \langle \cos\ \theta_n \rangle \geq 0 \text{ and } \langle \sin\ \theta_n \rangle \geq 0 \\ L(\theta+\pi)/2\pi, & \text{if} \langle \cos\ \theta_n \rangle \leq 0 \\ L(\theta+2\pi)/2\pi, & \text{otherwise} \end{cases} \tag{17}$$

in which we first average $\cos\theta_n$ and $\sin\theta_n$ with ρ_n as the probability of weight

$$\langle \cos\ \theta_n \rangle = \sum_n \rho_n\ \cos(2\pi n/L), \tag{18}$$

$$\langle \sin\ \theta_n \rangle = \sum_n \rho_n\ \sin(2\pi n/L), \tag{19}$$

and then the average angular position θ of the center is calculated using

$$\theta = \arctan\left(\frac{\langle \sin\ \theta_n \rangle}{\langle \cos\ \theta_n \rangle}\right), \tag{20}$$

where the net charge density is $\rho_n = \rho_{n,n} - 1$. In order to distinguish the sign of the polarons, the site index n runs over the sites of the donor and acceptor, respectively. The parameter L represents the lattice number of each component. Furthermore, in order to display a good visualization of the dynamic results, we calculate the smoothed form of the lattice configuration for the displacement of each site and net charge density in the following:

$$\tilde{u}_n(t) = (-1)^n[2u_n(t) - u_{n-1}(t) - u_{n+1}(t)]/4, \tag{21}$$

$$\tilde{\rho}_n(t) = [2\rho_n(t) + \rho_{n-1}(t) + \rho_{n+1}(t)]/4. \tag{22}$$

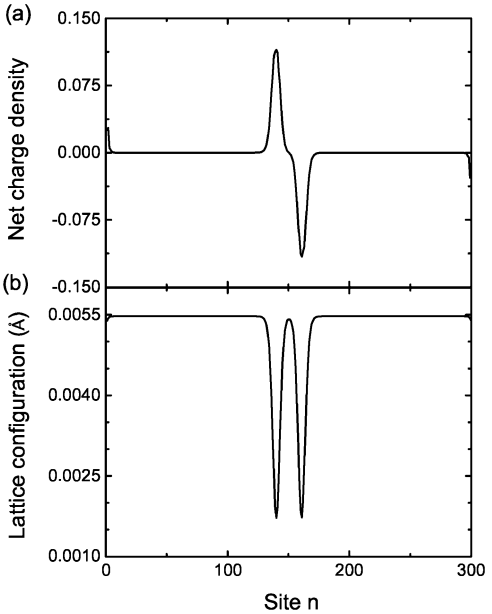

Fig. 2 (a) The net charge density of the CT state and (b) the lattice configuration for the site displacements with $W = 60a_0$, $V_0 = 0.03$ eV, $U = 0.02$ eV and a_0 being the lattice constant.

As an example of the emergence of the CT state, we show in Fig. 2 the case of $W = 60a_0$, $V_0 = 0.03$ eV and $U = 0.02$ eV. Two localized states of electrons in a CT state are observed clearly, which correspond to two oppositely charged polarons, as shown in Fig. 2(a). As stated above, these two localized electronic states can induce two local lattice distortions on the molecular chain, which is presented in Fig. 2(b). These two polarons interact with each other *via* both the self-trapping valleys and the Coulomb interaction, and the shorter the distance, d, between them is, the stronger the effective binding energy is. Here, the distance, d, is quantified by the difference in charge centers between the two polarons, *i.e.*, $d = \Delta x_c$. When d is shorter than a critical value, d_c, the attractive interaction in between would pull the two polarons together and merge them into a single self-trapping valley to form a Frenkel exciton, and in this situation the CT state can not be robustly formed. Therefore, the emergence of a robust CT state naturally refers to the value of d_c, which strongly depends on the interfacial width, W, the molecular ESP drop, V_0, and the Coulomb interaction, U. In addition, the molecular ESP drop, V_0, acts as a driving energy to dissociate the CT state, and when V_0 is too strong the polaron itself is not stable, so is the CT state.

Fig. 3 displays d_c at different V_0 for three values of interfacial width, W, with $U = 0.02$ eV. There are small fluctuations stemming from numerical errors since the driving force is very

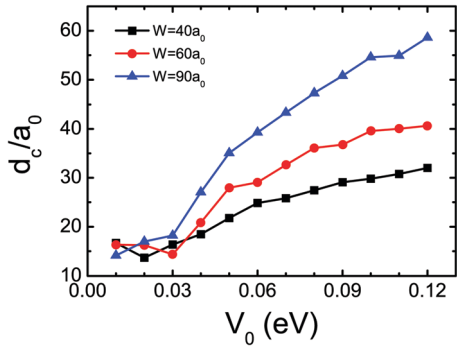

Fig. 3 The critical value of distance, d_c, between two oppositely charged polarons *versus* the molecular ESP drop, V_0, for three interfacial widths with U = 0.02 eV.

flat in a large extent of parameters. It is shown that the narrower interfacial layer is more helpful to facilitate the formation of a robust CT state with a shorter distance, d_c. Moreover, when V_0 is smaller than 0.03 eV, the critical distance, d_c, changes slightly, indicating that the binding and the driving energy are easy to balance in this case and the d_c of $\sim$14 lattice sites is minimally needed to form a CT state. As V_0 increases from 0.03 eV to 0.12 eV, d_c increases as well to weaken the electric field and balance the binding energy. It is also found that when V_0 is larger than 0.13 eV, the system cannot spontaneously form two localized polarons no matter how wide the interface is, suggesting that the ESP drop is too large to induce a stable polaron state. We also observe that the maximum value of the molecular ESP drop, V_0^m, for the emergence of the CT state is sensitive to the Coulomb interaction, U: the stronger the interaction is, the larger the V_0^m is. Fig. 4 shows that V_0^m increases almost linearly as U increases, further corroborating the scenario above. Experimentally, the ionic potentials of PDCBT-2F and IT-4F are measured using UPS and the results are -5.55 and -5.68 eV, respectively, with the difference being also 0.13 eV.[41] Although the system we are studying is different, the core moieties are quite similar. Hence, we can conclude here that the question of whether a CT state is formed in all-PSCs is parametrized in our model, which can be quantitatively examined with further experimental research.

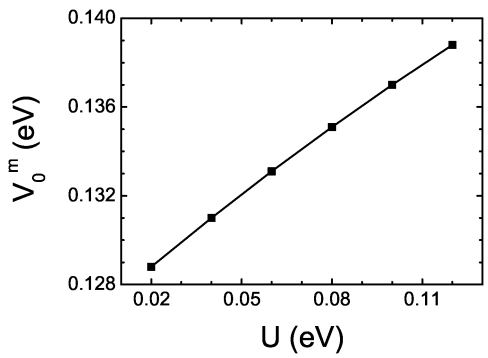

Fig. 4 The maximum value of molecular ESP drop, V_0^m, for the formation of a stable CT state *versus* the Coulomb interaction, U, with $W = 60a_0$.

The dynamics of the CT state are simulated *via* the non-adiabatic dynamic method at different interfacial widths from $10a_0$ to $120a_0$ with V_0 = 0.03 eV, and U = 0.02 eV. The initial distance between the two oppositely charged polarons is set to be around d_c, namely, the minimum size of the CT state. In detail, the two polarons initially reside on sites 142 and 158, respectively, so the initial size of the CT state is set to $16a_0$. As displayed in Fig. 5(a) and (b), following time evolution, the two polarons move separately along the chain enabled by the driving force provided by the ESP drop at the D/A interface. With increasing distance between them, the Coulomb attraction of these two polarons tends to be weak until it can be ignored when the two polarons are far enough away from each other. The current interest is then, how to determine the dissociation of the CT state given the dynamics of the two oppositely charged polarons. According to the Onsager theory,[60] when the Coulomb attraction between the two polarons is equal to or smaller than the thermal energy k_BT at room temperature, the two polarons can be regarded to dissociate, namely the CT state dissociates into free polarons giving rise to the generation of a photocurrent.

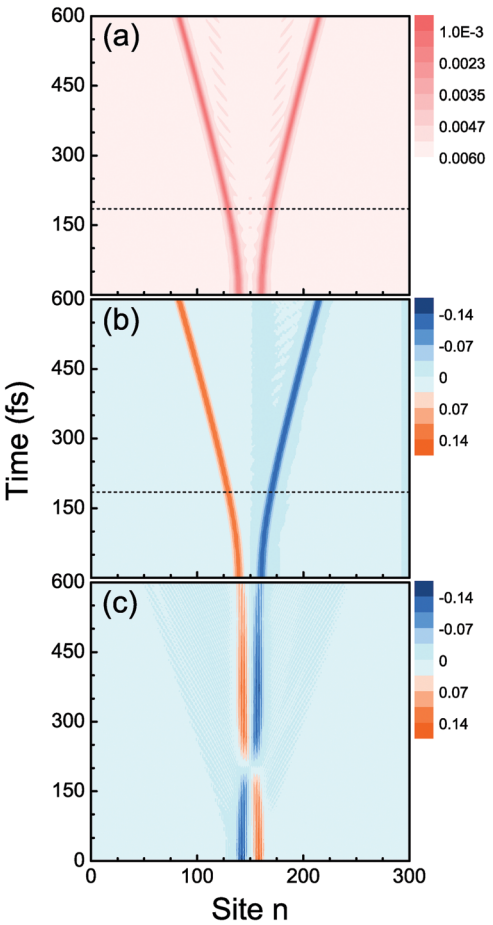

Fig. 5 Time evolution of (a) the lattice configuration $\tilde{u}_n(t)$ and (b) the net charge density $\tilde{\rho}_n(t)$ for CT state dissociation at the D/A interface with V_0 = 0.03 eV. (c) The net charge density $\tilde{\rho}_n(t)$ with V_0 = 0. The other parameters are: $W = 60a_0$ and U = 0.02 eV. The dashed lines indicate the dissociation time of CT state.

The distance at which the two polarons are regarded to be free is the so-called Coulomb capture radius, defined as

$$R_c = \frac{e^2}{4\pi\varepsilon_r\varepsilon_0 k_B T}, \quad (23)$$

where e is the elementary charge of an electron, ε_r is the relative dielectric constant, ε_0 is the permittivity of a vacuum, k_B is Boltzmann's constant and T is temperature. For most organic molecules and polymers, the dielectric constant ranges between 3 and 4,[19] so we can simply set it to 3.5. The Coulomb capture radius, R_c, is then calculated to be around 160 Å (*i.e.*, $\sim 40a_0$) in our case. By this definition, we can find that the dissociation time T_D of the CT state, defined as the time point that the distance between the two polarons is equal to R_c, is found to be $\sim$190 fs, denoted by the dashed line in Fig. 5, with the interfacial width being $60a_0$, suggesting that the CT state dissociation takes place in an ultrafast timescale. The results for $V_0 = 0$ are also displayed in Fig. 5(c). Compared to Fig. 5(b), Fig 5(c) shows a different situation where the two oppositely charged polarons cannot separate but solely oscillate around the initial site while time evolving. This is easy to understand since the driving force, *i.e.* ESP drop, is absent in the system.

A suitable interface for efficient dissociation in the D/A heterojunction is crucial to the efficiency of OSCs. The experiments have revealed that the dissociation of the CT state is sensitive to the scale of the phase separation of D/A blend films in non-fullerene cells.[61–63] It is thus interesting to make a comparison of the dissociation time T_D among various interfacial widths, which is shown in Fig. 6. With increasing interfacial width, the dissociation time dramatically decreases when $W < 60a_0$ followed by a slow increase. When the interface has a relatively small width of $10a_0$, the CT state takes $\sim$490 fs to dissociate. This is because in the initial state the two polarons are partly located outside the interfacial region and do not feel the driving force induced by the ESP drop very much. It is obvious that the dissociation of the CT state inside the interfacial region is much more efficient than that outside the interface. When the interfacial width is larger than $60a_0$, the two polarons completely reside in the interfacial region, but the electric field and thus the driving force induced by the ESP drop become smaller, leading to the slow dissociation of the CT state. Consequently, the optimum value of the interfacial width for an efficient dissociation time is determined to be $60a_0$ ($\sim$23 nm) in our case, which is actually a typical value in experiments. For example, the scale of phase separation of D/A blend films is reported to be 10–25 nm in J51/N2200-based cells,[6] J91/m-ITIC-based cells,[49] PJ2/IDIC-based cells,[50] and PTB7-Th/PDI-V-based cells.[64] Despite the quantitative difference in the realistic solar cells, the interfacial width of around $60a_0$ dominated by the phase separation of two polymer chains in the heterojunction structure is the most favorable for the dissociation of the CT state, in good agreement with the experimental results.[6,49,50,64]

One would think that when we discuss an ultrafast process for the dissociation of the CT state, the introduction of the Coulomb capture radius based on the thermal fluctuation at room temperature does not make sense. It is thus contributive to give a more enlightening measure for the dissociation based upon the quantum dynamics. Let us ask, if the two polarons in the CT state and also the two separated ones are regarded as two different partites, how do we identify the quantum correlations between these two quantum states? The quantum trace distance is one of the extensively used measures that distinguish two quantum states accurately, which can be expressed as[65–67]

$$D(\rho, \Omega) = \frac{1}{2}\mathrm{Tr}\sqrt{(\rho-\Omega)^\dagger(\rho-\Omega)}, \quad (24)$$

where Ω denotes the density matrix of the initial CT state and ρ represents the instantaneous density matrix of the system at time t. To this end, the quantum trace distance is introduced to quantify the dissociation as shown in Fig. 7. As a comparison, Fig. 7(a) first displays the time evolution of the spatial distance between two polarons. With increasing time, the spatial distance,

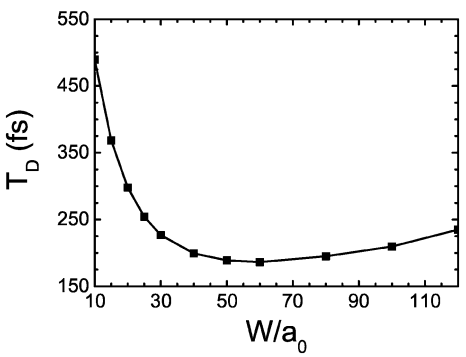

Fig. 6 The dissociation time, T_D, of the CT state (see the text for the definition) *versus* the interfacial width.

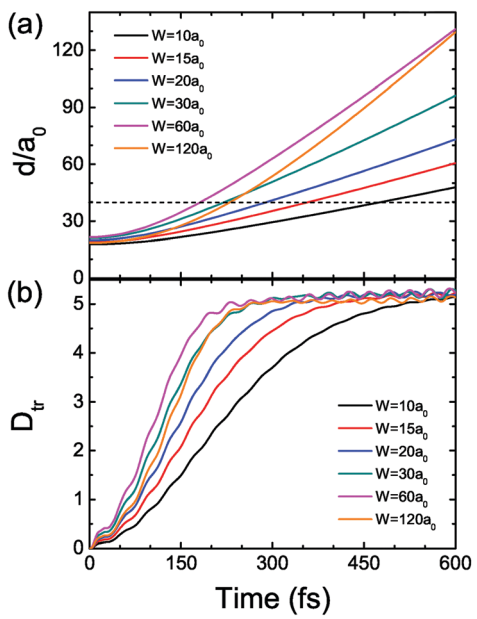

Fig. 7 Time evolution of (a) the spatial distance, d, between two polarons and (b) the trace distance, D_{tr}, for CT state dissociation for various interfacial widths. The dashed line reflects the Coulomb capture radius, R_c.

d, increases approximately linearly for all interfacial widths and $W = 60a_0$ is the optimum value for the efficient dissociation of the CT state, as discussed above. Fig. 7(b) exhibits the time evolution of the trace distance in the dissociation process of the CT state. Despite the difference in interfacial width, the trace distance, D_{tr}, behaves similarly. Namely, it firstly increases with increasing time and afterward remains approximately constant, suggesting that the quantum coherence between the two polarons vanishes. It is found that the time point at which the trace distance is constant, namely where the two polarons completely lose coherence, exhibits significant differences for various interfacial widths. Coherence is completely lost most quickly when the interfacial width is $60a_0$. Below this value, the time gets significantly longer. The narrower the interface is, the longer the time is. Comparing with Fig. 7(a), we can find that the time of the dissociation of the CT state based upon the Coulomb capture radius is close to that for losing the coherence at different interfacial widths. Losing the coherence means changing from a quantum scenario to a classical scenario, so this implies that the dissociation of the CT state manifests a decoherence scenario, and in a quantitative manner the classical distance between polarons can serve as a featured measure of the dissociation, accompanying the quantum trace distance. Subsequently, the quantum trace distance is highly recommended to the community for fingerprinting the ultrafast charge separation in OSCs.

IV. Conclusions

In this work, we theoretically investigated the formation and dynamic dissociation of the CT state at the D/A interface. We modified the extensively used SSH model with a molecular ESP drop and performed the simulations with the non-adiabatic dynamic method. It was found that the formation of the CT state depends on the width of the interfacial layer, the ESP drop between the interfacial layer and the Coulomb interaction. A maximum ESP drop for the robust formation of the CT state was observed. The dynamic dissociation process of the CT state was then discussed. With the Coulomb capture radius being the criterion, it was found that the two oppositely charged polarons in the CT state separate completely at the D/A interface within hundreds of femtosecond. The D/A interface of 23 nm was the most suitable interfacial layer for the dissociation of the CT state. In addition, the quantum trace distance provided a further demonstration of the dissociation of the CT state, which can explain the physical meaning of charge separation properly at the D/A interface. Our work can be of practical significance to the optimization of all-PSCs.

Before the end, we would like to have more discussion on the mechanisms of charge separation. Fullerene molecules possess very high symmetry, so the degeneracy of electronic states is larger than that in other acceptors and the wavefunctions are more likely to be delocalized due to the apparent translational symmetry. Both the delocalization and entropy arguments are frequently employed to interpret the ultrafast charge separation in fullerene-based cells as addressed in the Introduction section. These arguments were also applied to non-fullerene cells, as for example Friend's group observed a ballistic charge separation within 200 fs.[68] Regardless of this finding, one still has to comprehend the fact that a number of non-fullerene acceptors are working very well in state-of-the-art cells and not all of them hold high symmetry and delocalized electronic wavefunctions. Moreover, the small driving force is always a big issue for charge separation in non-fullerene cells.[28] These facts turned out to be the motivation of our previous and present mechanical research.[42,44] The role of entropy in different types of non-fullerene cell will also constitute to our future work.

Conflicts of interest

There are no conflicts to declare.

Acknowledgements

The authors gratefully acknowledge support from the National Natural Science Foundation of China (Grant No. 11574052 and 91833305).

References

1 Y. Lin, J. Wang, Z.-G. Zhang, H. Bai, Y. Li, D. Zhu and X. Zhan, *Adv. Mater.*, 2015, **27**, 1170–1174; Y. Lin, Z.-G. Zhang, H. Bai, J. Wang, Y. Yao, Y. Li, D. Zhu and X. Zhan, *Energy Environ. Sci.*, 2015, **8**, 610–616.
2 L. Meng, Y. Zhang, X. Wan, C. Li, X. Zhang, Y. Wang, X. Ke, Z. Xiao, L. Ding, R. Xia, H.-L. Yip, Y. Cao and Y. Chen, *Science*, 2018, **361**, 1094–1098.
3 J. Hou, O. Inganäs, R. H. Friend and F. Gao, *Nat. Mater.*, 2018, **17**, 119.
4 Z.-G. Zhang, Y. Yang, J. Yao, L. Xue, S. Chen, X. Li, W. Morrison, C. Yang and Y. Li, *Angew. Chem., Int. Ed.*, 2017, **56**, 13503–13507.
5 X. Liu, Y. Yan, Y. Yao and Z. Liang, *Adv. Funct. Mater.*, 2018, **28**, 1802004.
6 L. Gao, Z.-G. Zhang, L. Xue, J. Min, J. Zhang, Z. Wei and Y. Li, *Adv. Mater.*, 2016, **28**, 1884–1890.
7 B. Fan, L. Ying, Z. Wang, B. He, X.-F. Jiang, F. Huang and Y. Cao, *Energy Environ. Sci.*, 2017, **10**, 1243–1251; B. Fan, L. Ying, P. Zhu, F. Pan, F. Liu, J. Chen, F. Huang and Y. Cao, *Adv. Mater.*, 2017, **29**, 1703906; Z. Li, L. Ying, R. Xie, P. Zhu, N. Li, W. Zhong, F. Huang and Y. Cao, *Nano Energy*, 2018, **51**, 434–441.
8 C. Yang, H. Park, S. Chen, S. Jung, H. J. Cho, N.-H. Kim, S. Jung, J. Xu, J. Oh, Y. Cho, H. Kim, B. Lee, Y. An, C. Zhang, M. Xiao, H. Ki, Z.-G. Zhang, J.-Y. Kim and Y. Li, *Angew. Chem., Int. Ed.*, 2018, **57**, 1–7.
9 C. Mu, P. Liu, W. Ma, K. Jiang, J. Zhao, K. Zhang, Z. Chen, Z. Wei, Y. Yi, J. Wang, S. Yang, F. Huang, A. Facchetti, H. Ade and H. Yan, *Adv. Mater.*, 2014, **26**, 7224–7230.
10 N. Zhou, A. S. Dudnik, T. I. Li, E. F. Manley, T. J. Aldrich, P. Guo, H. C. Liao, Z. Chen, L. X. Chen, R. P. Chang,

A. Facchetti, M. Olvera de la Cruz and T. J. Marks, *J. Am. Chem. Soc.*, 2016, **138**, 1240–1251.
11 Z. Li, X. Xu, W. Zhang, X. Meng, W. Ma, A. Yartsev, O. Inganäs, M. R. Andersson, R. A. J. Janssen and E. Wang, *J. Am. Chem. Soc.*, 2016, **138**, 10935–10944.
12 A. Facchetti, *Mater. Today*, 2013, **16**, 123–132.
13 H. Kang, W. Lee, J. Oh, T. Kim, C. Lee and B. J. Kim, *Acc. Chem. Res.*, 2016, **49**, 2424–2434.
14 N. Zhou and A. Facchetti, *Mater. Today*, 2018, **21**, 377–390.
15 K. Zhang, R. Xia, B. Fan, X. Liu, Z. Wang, S. Dong, H.-L. Yip, L. Ying, F. Huang and Y. Cao, *Adv. Mater.*, 2018, **30**, 1803166.
16 J. J. M. Halls, C. A. Walsh, N. C. Greenham, E. A. Marseglia, R. H. Friend, S. C. Moratti and A. B. Holmes, *Nature*, 1995, **376**, 498–500.
17 R. H. Friend, D. D. C. Bradley and P. D. Townsend, *J. Phys. D: Appl. Phys.*, 1987, **20**, 1367–1384.
18 M. Chandross, S. Mazumdar, S. Jeglinski, X. Wei, Z. V. Vardeny, E. W. Kwock and T. M. Miller, *Phys. Rev. B: Condens. Matter Mater. Phys.*, 1994, **50**, 14702–14705.
19 V. I. Arkhipov and H. Bässler, *Phys. Status Solidi A*, 2004, **201**, 1152–1187.
20 M. Muntwiler, Q. Yang, W. A. Tisdale and X.-Y. Zhu, *Phys. Rev. Lett.*, 2008, **101**, 196403.
21 J. L. Brédas, J. E. Norton, J. Cornil and V. Coropceanu, *Acc. Chem. Res.*, 2009, **42**, 1691–1699.
22 X. Y. Zhu, Q. Yang and M. Muntwiler, *Acc. Chem. Res.*, 2009, **42**, 1779–1787.
23 Z. Sun and S. Stafström, *J. Chem. Phys.*, 2013, **138**, 164905.
24 K. Gao, S. Xie, S. Yin and D. Liu, *Org. Electron.*, 2011, **12**, 1010–1016.
25 E. R. Bittner, J. G. S. Ramon and S. Karabunarliev, *J. Chem. Phys.*, 2005, **122**, 214719.
26 H. Tamura, E. R. Bittner and I. Burghardt, *J. Chem. Phys.*, 2007, **126**, 021103.
27 B. P. Rand, D. P. Burk and S. R. Forrest, *Phys. Rev. B: Condens. Matter Mater. Phys.*, 2007, **75**, 115327.
28 J. Liu, S. Chen, D. Qian, B. Gautam, G. Yang, J. Zhao, J. Bergqvist, F. Zhang, W. Ma, H. Ade, O. Inganäs, K. Gundogdu, F. Gao and H. Yan, *Nat. Energy*, 2016, **1**, 16089.
29 V. C. Nikolis, J. Benduhn, F. Holzmueller, F. Piersimoni, M. Lau, O. Zeika, D. Neher, C. Koerner, D. Spoltore and K. Vandewal, *Adv. Energy Mater.*, 2017, **7**, 1700855.
30 L. Sebastian and G. Weiser, *Phys. Rev. Lett.*, 1981, **46**, 1156.
31 O. Rubel, S. D. Baranovskii, W. Stolz and F. Gebhard, *Phys. Rev. Lett.*, 2008, **100**, 196602.
32 T. Strobel, C. Deibel and V. Dyakonov, *Phys. Rev. Lett.*, 2010, **105**, 266602.
33 C. Deibel, T. Strobel and V. Dyakonov, *Phys. Rev. Lett.*, 2009, **103**, 036402.
34 B. A. Gregg, *J. Phys. Chem. Lett.*, 2011, **2**, 3013–3015.
35 F. Gao, W. Tress, J. Wang and O. Inganäs, *Phys. Rev. Lett.*, 2015, **114**, 128701.
36 N. R. Monahan, K. W. Williams, B. Kumar, C. Nuckolls and X. Y. Zhu, *Phys. Rev. Lett.*, 2015, **114**, 247003.
37 S. Ono and K. Ohno, *Phys. Rev. B*, 2016, **94**, 075305.
38 L. Ye, X. Jiao, W. Zhao, S. Zhang, H. Yao, S. Li, H. Ade and J. Hou, *Chem. Mater.*, 2016, **28**, 6178–6185.
39 B. R. Gautam, C. Lee, R. Younts, W. Lee, E. Danilov, B. J. Kim and K. Gundogdu, *ACS Appl. Mater. Interfaces*, 2015, **7**, 27586–27591.
40 K. Zhou, R. Zhang, J. Liu, M. Li, X. Yu, R. Xing and Y. Han, *ACS Appl. Mater. Interfaces*, 2015, **7**, 25352–25361.
41 H. Yao, D. Qian, H. Zhang, Y. Qin, B. Xu, Y. Cui, R. Yu, F. Gao and J. Hou, *Chin. J. Chem.*, 2018, **36**, 491–494.
42 Y. Yao, X. Xie and H. Ma, *J. Phys. Chem. Lett.*, 2016, **7**, 4830–4835.
43 Y. Yao, K. W. Sun, Z. Luo and H. Ma, *J. Phys. Chem. Lett.*, 2018, **9**, 413–419.
44 Y. Yao, *J. Chem. Phys.*, 2018, **149**, 194902.
45 W. P. Su, J. R. Schrieffer and A. J. Heeger, *Phys. Rev. Lett.*, 1979, **42**, 1698; *Phys. Rev. B: Condens. Matter Mater. Phys.*, 1980, **22**, 2099.
46 H. Bin, L. Gao, Z.-G. Zhang, Y. Yang, Y. Zhang, C. Zhang, S. Chen, L. Xue, C. Yang, M. Xiao and Y. Li, *Nat. Commun.*, 2016, **7**, 13651.
47 B. Qiu, L. Xue, Y. Yang, H. Bin, Y. Zhang, C. Zhang, M. Xiao, K. Park, W. Morrison, Z.-G. Zhang and Y. Li, *Chem. Mater.*, 2017, **29**, 7543–7553.
48 H. Bin, Y. Yang, Z.-G. Zhang, L. Ye, M. Ghasemi, S. Chen, Y. Zhang, C. Zhang, C. Sun, L. Xue, C. Yang, H. Ade and Y. Li, *J. Am. Chem. Soc.*, 2017, **139**, 5085–5094.
49 L. Xue, Y. Yang, J. Xu, C. Zhang, H. Bin, Z.-G. Zhang, B. Qiu, X. Li, C. Sun, L. Gao, J. Yao, X. Chen, Y. Yang, M. Xiao and Y. Li, *Adv. Mater.*, 2017, **29**, 1703344.
50 S. Chen, S. M. Lee, J. Xu, J. Lee, K. C. Lee, T. Hou, Y. Yang, M. Jeong, B. Lee, Y. Cho, S. Jung, J. Oh, Z.-G. Zhang, C. Zhang, M. Xiao, Y. Li and C. Yang, *Energy Environ. Sci.*, 2018, **11**, 2569–2580.
51 M. Jeong, S. Chen, S. M. Lee, Z. Wang, Y. Yang, Z.-G. Zhang, C. Zhang, M. Xiao, Y. Li and C. Yang, *Adv. Energy Mater.*, 2018, **8**, 1702166.
52 The hopping integrals t_0 for both J51 and N2200 were calculated to be around 0.09 eV using our quantum chemistry computations. The parameters for the lattice part can be determined by considering the relevant vibrational spectra. For N2200, *e.g.*, the primary bare optical phonon mode ω_Q is 1769 cm^{-1}, so that K can be calculated as $M\omega_Q^2/4 = 231$ eV $Å^{-2}$. The reorganization energy is 0.018 eV with respect to the relevant spectra, so that α is determined to be 3.4 eV $Å^{-2}$ as the equilibrated $|u_n - u_{n-1}|$ is calculated to be 0.00545 Å. a_0 is the mean distance between the cores of thiophene ring. U and V_0 are adjustable parameters.
53 D. Wang, L. Chen, R. Zheng, L. Wang and Q. Shi, *J. Chem. Phys.*, 2010, **132**, 081101; L. Wang, D. Beljonne, L. Chen and Q. Shi, *J. Chem. Phys.*, 2011, **134**, 244116.
54 Y. Ono and A. Terai, *J. Phys. Soc. Jpn.*, 1990, **59**, 2893–2904.
55 C. da Silva Pinheiro and G. M. e Silva, *Phys. Rev. B: Condens. Matter Mater. Phys.*, 2002, **65**, 094304.
56 M. P. Lima and G. M. e Silva, *Phys. Rev. B: Condens. Matter Mater. Phys.*, 2006, **74**, 224304.
57 W. F. da Cunha, L. A. R. Junior, R. Gargano and G. M. e Silva, *Phys. Chem. Chem. Phys.*, 2014, **16**, 17072–17080.

58 M. R. Mahani, A. Mirsakiyeva and A. Delin, *J. Phys. Chem. C*, 2017, **121**, 10317–10324.
59 L. A. Ribeiro, P. H. Oliveira Neto, W. F. da Cunha, L. F. Roncaratti, R. Gargano, D. A. da Silva Filho and G. M. e Silva, *J. Chem. Phys.*, 2011, **135**, 224901.
60 L. Onsager, *Phys. Rev.*, 1938, **54**, 554.
61 C. R. McNeill, *Energy Environ. Sci.*, 2012, **5**, 5653–5667.
62 Y. Zhou, T. Kurosawa, W. Ma, Y. Guo, L. Fang, K. Vandewal, Y. Diao, C. Wang, Q. Yan, J. Reinspach, J. Mei, A. L. Appleton, G. I. Koleilat, Y. Gao, S. C. Mannsfeld, A. Salleo, H. Ade, D. Zhao and Z. Bao, *Adv. Mater.*, 2014, **26**, 3767–3772.
63 N. D. Eastham, J. L. Logsdon, E. F. Manley, T. J. Aldrich, M. J. Leonardi, G. Wang, N. E. Powers-Riggs, R. M. Young, L. X. Chen, M. R. Wasielewski, F. S. Melkonyan, R. P. H. Chang and T. J. Marks, *Adv. Mater.*, 2018, **30**, 1704263.
64 Y. Guo, Y. Li, O. Awartani, J. Zhao, H. Han, H. Ade, D. Zhao and H. Yan, *Adv. Mater.*, 2016, **28**, 8483–8489.
65 C. A. Fuchs and J. Van De Graaf, *IEEE Trans. Inf. Theory*, 1999, **45**, 1216–1227.
66 H.-P. Breuer, E.-M. Laine and J. Piilo, *Phys. Rev. Lett.*, 2009, **103**, 210401.
67 B. Aaronson, R. L. Franco, G. Compagno and G. Adesso, *New J. Phys.*, 2013, **15**, 093022.
68 Y. Tamai, Y. Fan, V. O. Kim, K. Ziabrev, A. Rao, S. Barlow, S. R. Marder, R. H. Friend and S. M. Menke, *ACS Nano*, 2017, **11**, 12473–12481.